Applied Energy 309 (2022) 118441

Contents lists available at ScienceDirect

Applied Energy

journal homepage: www.elsevier.com/locate/apenergy

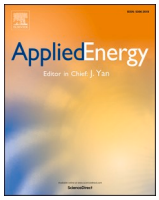

A novel rolling optimization strategy considering grid-connected power fluctuations smoothing for renewable energy microgrids

Shenglin Li, Jizhong Zhu *, Hanjiang Dong, Haohao Zhu, Junwei Fan

School of Electric Power Engineering, South China University of Technology, Guangzhou 510641, China

HIGHLIGHTS

- A rolling optimization strategy is proposed for microgrid operation optimization.
- Flexible load and hybrid energy storage are applied jointly to power regulation.
- A priority-based power fluctuations smoothing method is first proposed.
- Energy trigger mechanism is designed to keep the optimal state of supercapacitor.

ARTICLE INFO

Keywords:
Microgrid
Renewable energy sources
Flexible load
Hybrid energy storage
Power fluctuations
Rolling optimization

ABSTRACT

The rise of microgrids provides an effective solution to the problem of local consumption of renewable energy sources. However, the power fluctuations are the crucial issue for the widespread adoption of the grid-connected microgrid with renewable energy sources. We aim to economically and locally solve the problem of grid-connected power fluctuations of microgrid. In this paper, a novel rolling optimization strategy considering grid-connected power fluctuations smoothing for microgrids is provided. Firstly, the mathematical model of the microgrid is described, which contains the grid-connected power limits and supercapacitor-battery hybrid energy storage system. Then, a priority-based smoothing method of power fluctuations is proposed for the first time. As a flexible load, the heating/cooling load is used as virtual energy storage to participate in power regulation. Finally, the rolling optimization strategy integrated with the energy trigger mechanism is designed to achieve the operation optimization. The objectives of this paper are to help the microgrids improve grid-connection friendliness and minimize the daily operating costs that include fluctuation penalties. Simulation results on different scenarios for a grid-connected microgrid show that the novel rolling optimization strategy has better performance in any scenario. Compared with the traditional strategy, the total operating costs of the proposed strategy can save 5.67% for a given scenario. We can conclude that the proposed rolling optimization strategy can effectively reduce cost payment and meet the requirement of grid-connected power fluctuations smoothing.

1. Introduction

As a substitute for fossil fuels, renewable energy sources (RESs) have been attracting more and more attention for their advantages, such as renewable and pollution-free. Except for the power supply, the literature [1] provided an effective way to exploit RESs, which investigates greenhouse heating by biogas, solar and ground energy. In a latest study [2], the distributed energy system with RESs is integrated into the Floating Production Storage and Offloading, which proves that the combination can reduce the part of carbon emission. Compared to 2010, the global weighted-average levelized cost of electricity of utility-scale solar photovoltaic (USD 0.068/kWh) and onshore wind (USD 0.053/kWh) in 2019 decreased by 82% and 39%, respectively [3]. These will have an impact on the widespread adoption of engineering applications. Microgrid (MG) is an emerging and promising technology since it can effectively promote the local consumption of distributed RESs. MG is defined as a small-scale power system [4], which generally consists of local load demand (LD), an energy storage system (ESS), and distributed generation (DG) units. DG units may include photovoltaic (PV), wind turbine (WT), diesel engine (DE) and so on. MG system is capable to operate in grid-connected and/or standalone modes [5]. Different from the traditional main grid, MG is close to the demand-side to complete power generation and consumption simultaneously.

* Corresponding author at: School of Electric Power Engineering, South China University of Technology, Guangzhou 510641, China.
E-mail address: zhujz@scut.edu.cn (J. Zhu).

https://doi.org/10.1016/j.apenergy.2021.118441
Received 6 October 2021; Received in revised form 15 November 2021; Accepted 23 December 2021
Available online 10 January 2022

Nomenclature

Acronyms

RESs	renewable energy sources
MG	microgrid
EMS	energy management system
PV	photovoltaic
WT	wind turbine
DE	diesel engine
HESS	hybrid energy storage system
SC	supercapacitor
HCL	heating/cooling load
CNL	conventional net load
SOC	state-of-charge
PFS	power fluctuations smoothing
TOU	time-of-use
DAOS	day-ahead optimization strategy
BROS	basic rolling optimization strategy
NROS	novel rolling optimization strategy
DOC	daily operation cost
APF	average power fluctuations

Sets and indices

t, T	index and number of optimization intervals
k, K	index and number of real-time intervals

Variables and Parameters

T^t_{in}, T^t_{out}	indoor and outdoor temperature
P^t_T	HCL power
F^t_D	fuel consumption of DE
$P_{D,r}$, P^t_D	rated power and output power of DE
u^t_D	binary state of DE
SOC^t_B	SOC of battery
$P^t_{B,ch}$	charging power of battery
$P^t_{B,dch}$	discharging power of battery
u^t_B	binary working state of battery
W^t_B	lifetime weighting factor of battery
SOC^t_S	SOC of SC
$P^t_{S,ch}$	charging power of SC
$P^t_{S,dch}$	discharging power of SC
u^t_S	binary working state of SC
C^t_S	SC degradation cost within time interval t
P^t_{LD}	total load demand
P^t_{CLD}	conventional load demand
P^t_{net}	conventional net load demand
$P^t_{G,B}$	power drawn from the main grid
$P^t_{G,S}$	power injected back to the main grid
$V^t_{G,B}$	TOU price bought from the main grid
$V^t_{G,S}$	TOU price sold back to the main grid
u^t_G	binary working state of grid power
$\Delta P^{2,t}_G$	square of the fluctuation of grid power

Solar generation and wind generation are intermittent, stochastic, and uncontrollable. Load demand can also be viewed as a variable social behavior [6]. Besides, load demand and RESs generation have different peak-valley characteristics. The negative effects of the natural source-load uncertainties in MG are mainly reflected in two aspects. In terms of the MG, the small-scale MG systems do not have enough ability to resist the strong and high-frequency power fluctuations. The random power fluctuations bring difficulties to the MG dispatching [7]. For the main grid, frequent power fluctuations generated by the grid-connected MGs may cause harmonic pollution and power quality problems.

Power electronic devices play an important role in the operation of grid-connected MGs. Specially, power electronic converters help to minimize harmonics and generate the required power [8]. In grid-connected mode, the PQ control strategy is recommended, whereas the V/f and Droop strategies are adopted when in standalone mode [9]. Unlike these studies, we focus on the energy management system (EMS) of the grid-connected MG with hybrid energy storage. We analyze and solve the problem of tie-line power fluctuations from the perspective of instantaneous power conservation. The EMS is helpful for the realization of MG operation with the goals of the economy [10], comfort [11], greenness [12], reliability [13], and so on. In the EMS of MGs, forecasting methods, scheduling strategy considering uncertainty and reasonable configuration of energy storage are the vital technologies for the energy management considering the grid-connected problems.

Power data forecast is a critical topic for the EMS of power system. Generally, power data that need to be predicted may include RESs output [14], load demand [15], and electricity price [16]. Depending on the types of predicted results, point prediction [17] and prediction intervals [18] are popularly applied in power forecasting. The method of prediction intervals with coverage probability is effective on forecast. However, we should be noted that these intrinsic uncertainties will still lead to inevitable prediction errors in spite of the most advanced forecasting methods.

The deterministic energy scheduling strategies in most previous research works [19] and [20], which didn't take into account power errors, are difficult to perform the expected optimization results. Thus, MGs have certain self-regulation ability to accommodate the power uncertainties is essential. There are several scheduling strategies to solve the MG uncertainties. For example, robust optimal dispatch [21] and probabilistic constrained approach [22] are two common approaches to deal with the forecast errors. In order to deal with the issue of uncertainties of power system, study [23] performed a reliability constraint stochastic model for unit commitment problem. Besides, Huang *et al.* [24] formulated a chance-constrained optimization problem to accommodate the uncertainties, and also presented a two-point estimate method-based particle swarm optimization to solve this problem. In literature [25], the event-driven automatic demand response framework was designed to deal with the uncertainties. Yang *et al.* [26] proposed a real-time EMS with a model predictive control-based dynamic optimization for MGs, which can deal with the data prediction errors. Compared with the above methods, the rolling optimization strategy is capable of feedback correction, which can make the MG system better to adapt the actual situation. In [27], a real-time scheduling optimization strategy with the rolling horizon was applied to reduce the impact of uncertainty on operation optimization. In the calculation of optimal dispatch, the above strategies are usually discrete time, but the actual operation is continuous. The discretization is another important reason for low-precision scheduling and power fluctuations.

Reasonable configuration of ESS can ensure stable and efficient operation both on the grid-side and the demand-side [28]. The battery-only ESS can also be used to mitigate the real-time power fluctuations. However, the battery still belongs to capital-intensive device, and the frequent charging/discharging operations may lead to serious degradation [29]. Due to the complementary between battery with high energy density and supercapacitor (SC) with high power density, the hybrid ESS (HESS) is generally used to gain economic benefits as well as smooth the instant power fluctuations. Compared with battery,

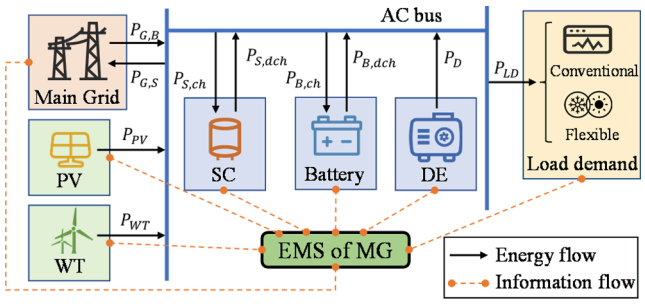

Fig. 1. The structure of a grid-connected microgrid.

supercapacitor can withstand a deeper depth of discharge and have a longer service life. Sharma *et al.* [30] pointed out that the HESS not only supported the steady state but also transient power changes. In the study [7], the proposed HESS with battery and ultracapacitor achieved load demand smoothing and RESs self-consumption without precise forecasting. Ju *et al.* [29] presented a two control layers-based EMS for MG with hybrid ESS, in which the supercapacitor compensated power mismatch in the lower layer, then the fluctuations caused by forecast errors were minimized. The energy capacity of SC is generally relatively small, and a suitable cooperation mechanism is needed to ensure the stable operation of SC. Besides, only a few works, which regard flexible loads as virtual energy storage to improve the operational economy. For example, due to the heating/cooling inertia of buildings in a short time, study [31] developed a virtual ESS-based building model to participate in the economic dispatch. However, the scheduling potential of flexible loads has not been used to smooth power fluctuations.

The peak-valley characteristics of RESs and load, the power prediction errors caused by uncertainties, and the time discretization in the optimization process are the main reasons for grid-connected power fluctuations. In the near future, more and more small and medium-scale microgrids will be integrated into the grid. If the MG is not capable of locally dealing with power fluctuations, the power fluctuations directly integrate to the distribution network, which can cause serious power quality problems. These approaches above contribute to mitigate the negative impact. However, most of the existing studies ignore the potential of power fluctuations smoothing by SC and flexible loads. Therefore, this paper focuses on economically and locally solving the problem of grid-connected power fluctuations of microgrid. The objectives of this paper are to help the microgrids improve grid-connection friendliness and minimize the daily operating costs. The main contributions of this paper are as follows:

1) A novel rolling optimization strategy considering grid-connected power fluctuations smoothing (PFS) is designed, which focuses on minimizing total operating costs and reducing grid-connected power fluctuations. Also, the mathematical model with different time resolutions is developed to accurately reflect the PFS process.
2) A priority-based smoothing method of power fluctuations is firstly proposed for smoothing unpredictable power fluctuations. In the proposed PFS method, a heating/cooling load is used as virtual energy storage, and it participates in power fluctuations smoothing together with the supercapacitor-battery hybrid ESS. In addition, the energy trigger mechanism is designed to keep the optimal state of supercapacitor.
3) The effectiveness of the proposed optimization strategy is analyzed. A typical MG consisting of solar-wind RESs, flexible load, hybrid ESS, and diesel engine is considered for simulation and discussion. Numerical results successfully demonstrate that the proposed strategy can effectively smooth the grid-connected power fluctuations and reduce cost payment.

The rest of this paper is organized as follows. The basic mathematical model of MG is described in Section 2. Section 3 proposed a novel rolling optimization strategy in detail. Case studies and results demonstrate the superiority of the proposed strategy in Section 4. Finally, Section 5 concludes the paper.

2. Mathematical model of grid-connected MG

A typical grid-connected microgrid (MG) including photovoltaic (PV), wind turbine (WT), diesel engine (DE), hybrid energy storage system (HESS), and load demand (LD) is considered in this paper. The MG can operate either in grid-connected mode with the main grid through the point of common coupling or in islanded mode. The structure of grid-connected MG is depicted in Fig. 1. An energy management system (EMS) is necessary to manage the energy flow and information flow for realizing the MG operation optimization. We first conduct a detailed mathematical modeling of each module of the microgrid in this chapter. Unless otherwise noted, we assume that MG is always left in grid-connected mode.

It should be noted that the mathematical modeling and the dispatching calculation are usually discrete time. Moreover, the deviation between the optimized scheduling results and the actual operation is unavoidable. A very small scheduling time resolution will increase the dispatching complexity, and may frequently cause switching work state and reduce their lifespan. Therefore, the scheduling models with different time resolutions can improve the scheduling accuracy.

Remark 1. Two different time indexes $t \in [1, 2, \cdots, T]$ and $k \in [1, 2, \cdots, K]$ are applied to formulate the MG scheduling model. 1) Optimization time resolution Δt is used for rolling optimization calculation. The modules involved in optimization include RESs outputs, load demand, DE, battery, and the main grid. 2) Real-time resolution Δk in each optimal time interval t is used to real-time smooth power fluctuations.

2.1. RESs and load demand

RESs-load bilateral uncertainties are the primary causes of unpredicted power fluctuations. In [6], PV power output depending on the incident solar irradiance and the PV cell temperature can be calculated by (1). WT energy capture depends on four factors: the free-stream air velocity, the air density, the swept area of the rotor, and the power coefficient [32]. The power generation of an operational WT is mainly determined by wind speed. In [33], the relationship between WT output power and wind speed can be calculated approximately by (2).

$$P_{PV} = P_{s,PV}\frac{G_a}{G_s}\left[1 + k\left(T_a + G_a\frac{NOCT - 20}{800} - T_r\right)\right] \tag{1}$$

$$P_{WT} = \begin{cases} 0, & v < v_{ci} \text{ or } v \geqslant v_{co} \\ P_{r,WT}\dfrac{v^3 - v_{ci}^3}{v_r^3 - v_{ci}^3}, & v_{ci} \leqslant v < v_r \\ P_{r,WT}, & v_r \leqslant v < v_{co} \end{cases} \tag{2}$$

where P_{PV} is PV power output and P_{WT} is WT power output. $P_{s,PV}$ and $P_{r,WT}$ are the PV maximum power and the rated power of a wind turbine. G_s and G_a are the irradiance under the standard test conditions and the incident solar irradiance. k is the temperature coefficient of the power, T_r and T_a are the reference temperature and the PV cell temperature. $NOCT$ is a nominal operating cell temperature. v, v_r, v_{ci}, and v_{co} are the current, rated, cut-in, and cut-out wind speeds, respectively.

The geographic location and climate are the long-term factors, which have a stable pattern and can be obtained through historical data. However, short-term weather factors such as wind speed, temperature, and irradiance are the main reasons for power fluctuations. It is difficult to obtain accurate power prediction results for RESs generation.

In addition, the energy consumption behavior of residents is usually

subjective and has limited control capabilities. According to the flexibility of scheduling time and operating power, the load demand can be divided into rigid load and flexible load [11]. In this paper, the flexible load with adjustable power is the first choice to smooth the unpredictable power fluctuations. Heating/cooling load (HCL) is a typical flexible load with heating/cooling inertia, which has the flexibility to adjust both time and power [34]. At the same time, HCL can be used as a virtual energy storage to participate in power regulation, which is ignored by most literatures. The indoor temperature should be controlled within a predefined range. In this paper, under the premise of meeting the temperature range, the HCL is applied to smooth power fluctuations in real time. The relationship among indoor temperature, outdoor temperature, and HCL power is described in (3) [24].

$$T_{in}^{t} = [T_{out}^{t-1} + (T_{in}^{t-1} - T_{out}^{t-1})e^{-\frac{\Delta t}{\tau}}] \pm R_T(1 - e^{-\frac{\Delta t}{\tau}})\cdot P_T^t \tag{3}$$

$$0 \leqslant P_T^t \leqslant P_{T,max} \tag{4}$$

$$T_{in,min} \leqslant T_{in}^t \leqslant T_{in,max} \tag{5}$$

where $T_{in,min}$ and $T_{in,max}$ are the predefined minimum and maximum indoor temperatures. $\tau = R_T C_{air}$, and R_T is the thermal resistance of building shell, C_{air} is heat capacity of indoor air, and $P_{T,max}$ is the maximum working power.

2.2. Diesel engine

The DE, which plays a role as backup supply due to the expensive generation costs, works only for power supply when MG is insufficient to maintain the normal operation. The relationship between the fuel consumption, rated power and output power can be approximated by several piecewise linear segments [35]. The fuel consumption of DE can be represented by Eq. (6). The DE cannot run at the no-load model, the power output needs to meet the constrain (7).

$$F_D^t = \Delta t\cdot(F_1\cdot P_{D,r}\cdot u_D^t + F_2\cdot P_D^t) \tag{6}$$

$$\theta_D\cdot P_{D,r} u_D^t \leqslant P_D^t \leqslant P_{D,r} u_D^t \tag{7}$$

where F_1 and F_2 are the intercept coefficient and the slope of fuel curve, respectively. Based on [36], they can be set to 0.08415 and 0.246, respectively. The binary variable u_D^t indicates that the state of the diesel engine (1 for working state). θ_D is the minimum power output coefficient.

There are some constraints that a diesel engine needs to follow during operation [21]. In Eqs. (8) and (9), the continuous working time is constrained to between the minimum and maximum uptime once the DE starts. The constraint about minimum downtime is given by Eq. (10) once the DE is shut down. In addition, the DE output power cannot be dramatically changed due to the technical restriction of the maximum electrical ramp rate in Eqs. (11) and (12).

$$\sum_{i=0}^{d_{on,u}/\Delta t} u_D^{t+i} \leqslant \frac{d_{on,u}}{\Delta t},\ t \in [1 - \frac{d_{on,u}}{\Delta t}, T - \frac{d_{on,u}}{\Delta t}] \tag{8}$$

$$\sum_{i=0}^{d_{on,l}/\Delta t - 1} u_D^{t+i} \geqslant \frac{d_{on,l}}{\Delta t}(u_D^t - u_D^{t-1}),\ t \in [2 - \frac{d_{on,l}}{\Delta t}, T - \frac{d_{on,l}}{\Delta t} + 1] \tag{9}$$

$$\sum_{i=0}^{\frac{d_{off,l}}{\Delta t}-1} (1 - u_D^{t+i}) \geqslant \frac{d_{off,l}}{\Delta t}(u_D^{t-1} - u_D^t),\ t \in [2 - \frac{d_{off,l}}{\Delta t}, T - \frac{d_{off,l}}{\Delta t} + 1] \tag{10}$$

$$P_D^t - P_D^{t-1} \leqslant u_D^t(1 - u_D^{t-1})(P_{D,r} - \Delta t\cdot P_{D,up,max}) + \Delta t\cdot P_{D,up,max} \tag{11}$$

$$P_D^{t-1} - P_D^t \leqslant u_D^{t-1}(1 - u_D^t)(P_{D,r} - \Delta t\cdot P_{D,dw,max}) + \Delta t\cdot P_{D,dw,max} \tag{12}$$

where $d_{on,l}$, $d_{on,u}$, and $d_{off,l}$ are the minimum uptime, maximum uptime, and minimum downtime, respectively. $P_{D,up,max}$ and $P_{D,dw,max}$ are the maximum lifting capacity and the maximum lowering capacity during one hour.

2.3. Hybrid energy storage system

The instability problem caused by the small-scale MG system can be alleviated by configuring ESS. SCs can not only respond to instantaneous power fluctuations, but also have a longer service life. Therefore, it is more economical to configure SC for smoothing unpredicted power fluctuations. In this paper, battery and supercapacitor are selected as the typical collaboration in HESS due to the complementary features.

1) *Operational model of battery*: The state-of-charge (SOC) is used to reflect the ratio of the current capacity to the rated capacity in energy storage. There is dynamic energy conservation between the charging and discharging operations, which is given in the reference [29]. The charging and discharging power of the battery must meet the power constraints for normal operation. In addition, the SOC should be limited within a specified range for preventing the battery from over-charged and over-discharged.

$$SOC_B^t = SOC_B^{t-1} + \Delta t\frac{P_{B,ch}^t\cdot\lambda_{B,ch} - P_{B,dch}^t \Big/ \lambda_{B,dch}}{C_B} \tag{13}$$

$$0 \leqslant P_{B,ch}^t \leqslant P_{B,ch,max}\cdot u_B^t \tag{14}$$

$$0 \leqslant P_{B,dch}^t \leqslant P_{B,dch,max}\cdot(1 - u_B^t) \tag{15}$$

$$SOC_{B,\min} \leqslant SOC_B^t \leqslant SOC_{B,\max} \tag{16}$$

where C_B is the rated capacity of the battery. $\lambda_{B,ch}$ and $\lambda_{B,dch}$ denote the charging efficiency and discharging efficiency. $P_{B,ch,\max}$ and $P_{B,dch,\max}$ are the allowable maximum charging and discharging power, respectively. The binary variable $u_B^t = 1$ means charging state, otherwise, it means discharging state or idle state. $SOC_{B,\min}$ and $SOC_{B,\max}$ are the allowable minimum SOC and maximum SOC.

Ignoring the impact on ambient temperature, the degradation cost of the battery is mainly affected by the depth of discharge and the value of power output. The lifetime weighting factor W_B^t associated with SOC is calculated by Eq. (17) [37]. The energy throughput method is introduced for defining the depreciation cost of the battery [36]. The battery is considered to have a fixed energy throughput and it can achieve the maximum value during its working life. Thus, the degradation cost C_B^{RH} in the given period can be described by Eq. (18).

$$W_B^t = \begin{cases} w_1, & \text{if} \quad 0 \leqslant SOC_B^t \leqslant 0.5 \\ w_2\cdot SOC_B^t + w_3, & \text{if} \quad 0.5 < SOC_B^t \leqslant 1 \end{cases} \tag{17}$$

$$C_B^{RH} = \frac{C_{B,inv}}{L_{B,thr}}\cdot\Delta t\sum_{t\in RH_T} W_B^t(P_{B,ch}^t + P_{B,dch}^t) \tag{18}$$

where $C_{B,inv}$ is the total investment cost of the battery. $L_{B,thr}$ is the total energy throughput. w_1, w_2, and w_3 are the coefficients of the lifetime weighting factor function. Based on the reference [37], the three coefficients are set as 1.3, −1.5, and 2.05.

2) *Operational model of SC*: The model of SC is similar to that of battery. In each optimization time interval $t \in RH_T$, the SC smooths the power fluctuations in real time. In this paper, the optimization time interval t is further divided into K real-time time intervals ($k \in RH_K = [1, 2, 3, \cdots, K]$). The duration of each real-time time interval Δk is equal to $\Delta t/K$. The operational model is presented below:

$$SOC_S^k = SOC_S^{k-1} + \Delta k \frac{P_{S,ch}^k \cdot \lambda_{S,ch} - P_{S,dch}^k \Big/ \lambda_{S,dch}}{C_S} \tag{19}$$

$$0 \leqslant P_{S,ch}^k \leqslant P_{S,ch,max} \cdot u_S^k \tag{20}$$

$$0 \leqslant P_{S,dch}^k \leqslant P_{S,dch,max} \cdot (1 - u_S^k) \tag{21}$$

$$SOC_{S,\min} \leqslant SOC_S^k \leqslant SOC_{S,\max} \tag{22}$$

where SOC_S^k and C_S are the SOC and the rated capacity of the SC. $P_{S,ch}^k$ and $P_{S,dch}^k$ indicate the charging power and discharging power. $\lambda_{S,ch}$ and $\lambda_{S,dch}$ denote the charging efficiency and discharging efficiency. $P_{S,ch,\max}$ and $P_{S,dch,\max}$ are the allowable maximum charging and discharging power, respectively. The binary variable $u_S^k = 1$ means charging state, otherwise, it means discharging state or idle state. $SOC_{S,\min}$ and $SOC_{S,\max}$ are the allowable minimum SOC and maximum SOC.

The exiting study [29] indicates that the degradation cost of SC is mostly related to working conditions such as temperature and terminal voltage. Moreover, the cycle life of SC is much longer than that of the battery. Its charging and discharging rates at a proper working condition have little effect on SC degradation. Therefore, in this paper, we assume that the SC lifetime is fixed, and the SC degradation cost C_S^t within an optimization time interval can be formulated by a linear function of time as follows:

$$C_S^t = \frac{C_{S,inv}}{24 \cdot 365 \cdot L_S} \cdot \Delta k \sum_{k \in RH_K} \text{sign}(P_{S,ch}^k + P_{S,dch}^k) \tag{23}$$

where $C_{S,inv}$ is the total investment cost of supercapacitor. L_S is the total working lifetime (year) of SC.

3. Proposed novel rolling optimization strategy

The bilateral uncertainties related to the RESs generation and load demand are usually difficult to predict accurately. Studies have shown that forecast errors are inevitable even with the most advanced forecasting methods [24]. In addition, although a smaller optimization time resolution can effectively improve scheduling accuracy, the time interval for optimization calculation is not infinitely small due to limited computing power. These are the two fundamental reasons for high-frequent unpredicted power fluctuations. Compared with the unpredictable high-frequent power fluctuations, the steady-state value predicted by point prediction methods can be used for scheduling optimization. However, the deterministic energy scheduling strategies usually ignore the existence of power errors. If the MG has no self-suppression ability, the predicted power errors can only be smoothed through the main grid for achieving the preset optimization results. As the number of microgrid increment, the significant ability of locally smoothing grid-connected power fluctuations can avoid harmonic pollution to the main grid.

In order to achieve our goal, we designed a novel rolling optimization strategy for energy management system in this section. Firstly, an energy trigger mechanism for SC is systematically given. Then, the operation optimization model of MG is fully presented. Next, a priority-based smoothing method of power fluctuations is design for solving the problem of grid-connected power fluctuations. Finally, an algorithm of novel ROS is well described in four parts. The following subsections will describe the proposed ROS in detail.

3.1. Energy trigger mechanism for SC

There are three uncertainties considered in the typical MG: the outputs of PV and WT, and load demand. Before launching dispatch optimization, it is necessary to predict the low-frequency component of the conventional net load (CNL) P_{net}^t, and it can be defined by Eq. (24).

$$\begin{cases} P_{LD}^t = P_{CLD}^t + P_T^t \\ P_{net}^t = P_{CLD}^t - \left(P_{PV}^t + P_{WT}^t\right) = P_{net,PP}^t - P_{net,error}^t \end{cases} \tag{24}$$

where $P_{net,PP}^t$ is the point prediction result of the CNL, and $P_{net,error}^t$ is the power error caused by forecast error and calculation discretization.

Generally, point prediction is responsible for predicting the stable value of the CNL, whereas the prediction intervals method is responsible for predicting the range of uncertainties. The coverage probability and the normalized root-mean-square width are used to evaluate the performance of prediction intervals. In a given period, the coverage probability is a probability $P(L^t \leq P_{net}^k \leq U^t)$, which means the target values are covered by the forecast range (between the lower bound L^t and upper bound U^t). Considering the limited space, this paper focuses on the research of optimization strategy. Thus, the prediction results are assumed to be known, and more details about the prediction method can be found in the work [38].

The SC is independent of optimization calculation, and it is served as a buffer to respond to unpredicted power fluctuations in real time. We can find that there is still a possibility that the accumulated energy of unpredictable power fluctuations exceeds the rated capacity of SC. Thus, an additional energy trigger mechanism is essential to maintain the SC in the optimal energy range. This trigger mechanism is more suitable for online ROS since the online self-correction function. The rule of the trigger mechanism for SC is made based on how far the SOC deviates from the optimal SOC, and the logical relationship of this rule is as follows:

The SOC deviation of SC δ_S is calculated in real-time.

$$\delta_S = SOC_S^0 - SOC_{S,opt} \tag{25}$$

where SOC_S^0 and $SOC_{S,opt}$ are the SOC of the previous time interval ($t = 0$) and the set optimal SOC, respectively. We need to set the trigger process according to the trigger threshold θ_S before the start of each rolling optimization.

If $\delta_S > \theta_S$, this indicates that the SC needs to be discharged. The first value of point prediction $P_{net,PP}^{t=1}$ is revised down, and reduced to close to the upcoming lower bound $L^{t=1}$. Similarly, if $\delta_S < -\theta_S$, this indicates that the SC needs to be charged. The first value of point prediction $P_{net,PP}^{t=1}$ is revised up, and increased to close to the upcoming upper bound $U^{t=1}$. The revised value of prediction result is presented below:

$$P_{net,PP}^{t=1} = \begin{cases} L^{t=1} + \xi_{PP} \cdot (U^{t=1} - L^{t=1}), & if\ \delta_S > \theta_S \\ U^{t=1} - \xi_{PP} \cdot (U^{t=1} - L^{t=1}), & if\ \delta_S < \theta_S \end{cases} \tag{26}$$

where $0 \leq \xi_{PP} < 0.5$ is the recovery coefficient for restoring the optimal state, which determines the SC recovery rate.

3.2. Operation optimization model of MG

Considering that the regular maintenance fee generated within the MG system is fixed and accounts for a small proportion of the total cost, we ignore the maintenance fee in the process of optimization calculation. In this paper, the objectives are to minimize the total daily operation costs and minimize grid-connected power fluctuations.

The total operation costs C_{TOC}^{RH} within RH consist of seven parts: the cost of energy transaction with the main grid C_G^{RH}, the operation cost of a diesel engine C_D^{RH}, the degradation cost of a battery C_B^{RH}, the penalty for grid-connected power fluctuations $C_{F,G}^{2,RH}$, the PV degradation cost C_{PV}^{RH}, the WT degradation cost C_{WT}^{RH}, and the degradation cost of supercapacitor C_S^{RH}.

Part of the grid-connected power fluctuations can be smoothed through optimal operation. The penalty term for grid-connected power fluctuations with the penalty factors ρ and ξ is defined by (30). The definition the square of the adjacent grid-connected power difference

helps to eliminate severe power fluctuations. The operation cost of DE consists of three parts: life loss cost, fuel consumption cost, and start-up cost.

$$C_{TOC}^{RH} = (C_G^{RH} + C_D^{RH} + C_B^{RH} + C_{F,G}^{2,RH}) + (C_{PV}^{RH} + C_{WT}^{RH} + C_S^{RH}) \tag{27}$$

$$C_G^{RH} = \Delta t \sum_{t \in RH_T} (P_{G,B}^t V_{G,B}^t - P_{G,S}^t V_{G,S}^t) \tag{28}$$

$$C_D^{RH} = \Delta t \frac{C_{D,inv}}{L_D} \sum_{t \in RH_T} u_D^t + V_{D,F} \sum_{t \in RH_T} F_D^t + V_{D,S} \sum_{t \in RH_T} u_D^t (1 - u_D^{t-1}) \tag{29}$$

$$C_{F,G}^{2,RH} = \rho(\xi_F \cdot \Delta P_G^{2,t=1} + \sum_{t \in [2,T]} \Delta P_G^{2,t}) \tag{30}$$

$$\Delta P_G^{2,t} = (P_{G,B}^t - P_{G,B}^{t-1})^2 + (P_{G,S}^t - P_{G,S}^{t-1})^2 \tag{31}$$

$$C_j^{RH} = C_{j,inv} \cdot \Delta t \cdot T / L_j, \quad j \in \{PV,\ WT\} \tag{32}$$

where $C_{D,inv}$ is the investment cost, L_D is the working lifetime, $V_{D,F}$ is the fuel price, and $V_{D,S}$ indicates a fixed start-up cost for DE. $C_{j,inv}$ and L_j are the total investment cost and working lifetime for PV or WT.

Moreover, the real-time power balance of the optimization model needs to be followed in each time interval. The constraints for peak power-limiting strategy are given by the main grid.

$$P_{net,PP}^t = P_{G,B}^t - P_{G,S}^t - P_T^t + P_D^t - P_B^t \tag{33}$$

$$P_B^t = P_{B,ch}^t - P_{B,dch}^t \tag{34}$$

$$0 \leqslant P_{G,B}^t \leqslant P_{G,B,max}^t \cdot u_G^t \tag{35}$$

$$0 \leqslant P_{G,S}^t \leqslant P_{G,S,max}^t \cdot (1 - u_G^t) \tag{36}$$

where $P_{G,B,max}^t$ and $P_{G,S,max}^t$ are the maximum buying power-limiting from the grid and the maximum selling power-limiting to the grid. The binary variable $u_G^t = 1$ indicates that the MG needs to buy power from the main grid.

According to the four various operating costs related to optimization process, the operation optimization model can be expressed as:

$$\begin{cases} min & Obj = C_G^{RH} + C_D^{RH} + C_B^{RH} + C_{F,G}^{2,RH} \\ s.t. & (3) - (18),\ (24) - (36) \\ variables: & \left\{P_T^t, P_{DE}^t, u_D^t, P_{B,ch}^t, P_{B,dch}^t, u_B^t, P_{G,B}^t, P_{G,S}^t, u_G^t\right\} \end{cases} \tag{37}$$

The input of the model (37) includes electricity price, power limits, CNL demand, outdoor temperature, technical and predefined parameters, and initial operating state. The output (or decision variables) of the model is optimal operation scheme for HCL, DE, battery, and grid-connected power. The objective function of the model is minimizing the four various operating costs related to the decision variables, and the constraints consist of the real-time power balance and the operational constraints of MG equipment.

3.3. Priority-based smoothing method of power fluctuations

In the proposed priority-based smoothing method of power fluctuations, heating/cooling load (top priority), supercapacitor (medium priority), and battery (low priority) are the three sequential energy sources that smooth the power error. As the HCL and battery participate in the MG optimization dispatch, we need to calculate the remaining power capacities of HCL and battery.

1) *Remaining power capacity*. The scheduling instructions $\{P_T^{t=1}, P_B^{t=1}\}$ of the first time interval are extracted from the rolling optimization results, and the remaining power capacities considering energy constraints for the heating/cooling load $P_{T,rem}^{t=1}$ and the battery $P_{B,rem}^{t=1}$ are counted.

- Heating/cooling load: Only one mode is allowed to work in the same time interval.

$$P_{T,min}^{t=1} - P_T^{t=1} \leqslant P_{T,rem}^{t=1} \leqslant P_{T,max}^{t=1} - P_T^{t=1} \tag{38}$$

$$P_{T,max}^{t=1} = \begin{cases} min\left\{\dfrac{T_{in,max} - T_{in}^0 e^{-\frac{\Delta t}{\tau}}}{R_T(1 - e^{-\frac{\Delta t}{\tau}})} - \dfrac{T_{out}^0}{R_T}, P_{T,max}\right\}, & \text{heating} \\ min\left\{\dfrac{T_{out}^0}{R_T} - \dfrac{T_{in,min} - T_{in}^0 e^{-\frac{\Delta t}{\tau}}}{R_T(1 - e^{-\frac{\Delta t}{\tau}})}, P_{T,max}\right\}, & \text{cooling} \end{cases} \tag{39}$$

$$P_{T,min}^{t=1} = \begin{cases} max\left\{\dfrac{T_{in,min} - T_{in}^0 e^{-\frac{\Delta t}{\tau}}}{R_T(1 - e^{-\frac{\Delta t}{\tau}})} - \dfrac{T_{out}^0}{R_T}, 0\right\}, & \text{heating} \\ max\left\{\dfrac{T_{out}^0}{R_T} - \dfrac{T_{in,max} - T_{in}^0 e^{-\frac{\Delta t}{\tau}}}{R_T(1 - e^{-\frac{\Delta t}{\tau}})}, 0\right\}, & \text{cooling} \end{cases} \tag{40}$$

- Battery

$$-P_{B,dch,max}^{t=1} - P_B^{t=1} \leqslant P_{B,rem}^{t=1} \leqslant P_{B,ch,max}^{t=1} - P_B^{t=1} \tag{41}$$

$$P_{B,ch,max}^{t=1} = min\left\{\frac{(SOC_{B,\max} - SOC_B^0)C_B}{\Delta t \cdot \lambda_{B,ch}}, P_{B,ch,max}\right\} \tag{42}$$

$$P_{B,dch,max}^{t=1} = min\left\{\frac{(SOC_B^0 - SOC_{B,\min})C_B \lambda_{B,dch}}{\Delta t}, P_{B,dch,max}\right\} \tag{43}$$

2) *Real-time smoothing by priority*. According to the set priority, the HCL is first used to smooth power fluctuations. When the power capacity of HCL is insufficient, SC and battery will be added. Note that the battery will only participate in the smoothing if there is a very large power fluctuations, and this is a small probability event. If none of them can work, only power fluctuations can be smoothed by the main grid.

3.4. Novel rolling optimization strategy

Since the time interval for optimization calculation is greater than the actual power fluctuations, the coordination between the power fluctuations smoothing and the scheduling optimization is necessary. The novel rolling optimization strategy (ROS) can correct various complex situations in the scheduling process in time. As a scheduling strategy with self-regulating ability, the ROS can effectively reduce the impact of errors by moving forward the rolling horizon and real-time correction [39].

Generally, there are three major parameters in the online rolling optimization as shown in Fig. 2. The rolling horizon (RH) determines the size of the rolling window or optimization horizon, and the moving interval (MI) indicates the time distance that the RH moves forward. Every time a MI passes, the rolling window moves forward with a MI. Since the periodic day and night alternation affects the renewable energy output and load demand, the RH is usually set to 24 h. In addition, the value of MI is an integer multiple of the time resolution. In particular, if MI is

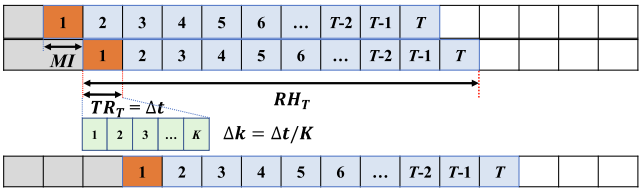

Fig. 2. Three major parameters of online rolling optimization strategy.

equal to 24 h, online rolling optimization will become day-ahead optimization. The smaller the MI value, the scheduling error can be corrected better in time. Therefore, this paper sets MI equal to Δt.

Algorithm 1. (*Novel rolling optimization strategy*)

Determine the fixed parameters of MG.
for each time interval t **do**
(Part 1: Data initialization and prediction)
Determine the time range of rolling horizon RH_T.
Update the state parameters: T_{in}^o, u_{DE}^o, P_{DE}^o, SOC_B^o, SOC_{SC}^o, P_G^o.
Predict CNL $P_{net,PP}^t$ and outdoor temperature T_{out}^t within RH.
(Part 2: Energy trigger mechanism for SC)
Flag = 0.
Calculate the SOC deviation of SC δ_{SC} by (25).
if $\delta_{SC} > \theta_{SC}$ or $\delta_{SC} < \theta_{SC}$**then**
Flag = 1.
Revise $P_{net,PP}^{t=1}$by (26).
end if
Update the forecast curve of CNL.
(Part 3: Optimization modeling and solution)
Construct operation optimization model within RH by (37).
Solve the optimization model by Gurobi 9.0 solver.
(Part 4: Module operation and real-time PFS)
Extract the optimal result of the first time interval.
Calculate the remaining power capacities of HCL and battery by (38-43).
if Flag == 0 **then**
Suppression resources = {HCL, SC, battery, grid}.
else then
Suppression resources = {SC, battery, grid}.
end if
Execute the MG optimal scheduling result. At the same time, the suppression resources are used to real-time suppression of power fluctuations according to the set priority.
end for

The novel ROS integrated with the designed energy trigger mechanism and the PFS method is shown in **Algorithm 1**, which is implemented by the EMS. It can be found that the novel ROS is mainly composed of four parts:

Part 1 (step 3–5): All parameters of the MG system are updated firstly, and the power data of the CNL and outdoor temperature within the rolling horizon is predicted.
Part 2 (step 6–12): The energy trigger mechanism for SC is performed and the forecast curve of CNL is updated.
Part 3 (step 13–14): The operation optimization model of MG is built and solved by Gurobi 9.0 solver.
Part 4 (step 15–22): The optimization result of the first time interval is performed, and the power fluctuations is smoothed by the priority-based PFS method in real time.

Remark 2. These four parts will be performed in each time interval. Noted that the ultimate solution of each module of MG will be obtained from the optimization result plus real-time smoothing operation.

4. Simulation results and discussions

To comprehensively illustrate the effectiveness of the proposed novel ROS, the novel ROS and the other two existing strategies [40] and [29] are simultaneously tested on a typical grid-connected MG, which is shown in Fig. 1. The MG system mainly consists of PV arrays (100 kW), wind turbines (50 kW), one diesel engine (20 kW), a HCL, and a HESS. The HESS based on battery and SC is considered for simulation and discussion. All numerical simulations are written in Python 3.8, and the solver chosen is Gurobi 9.0 [41].

In this Section, we will first make the simulation setups in which the six test scenarios and two new operation indicators for simulation studies are presented to illustrate the effectiveness of the proposed strategy. Then, we compared the optimized operation results of the three strategies under the small and large power fluctuations scenarios, respectively. Finally, we conducted a comprehensive analysis of the six test scenarios from the perspectives of economy and volatility.

Table 1
Time-of-use price of main grid.

Price type	Peak 11:00–22:00	Medium 08:00–11:00 22:00–24:00	Valley 00:00–08:00
Buying price ($/kWh)	0.20	0.10	0.05
Selling price ($/kWh)	0.12	0.06	0.03

Table 2
Basic parameters of microgrid.

Parameter	Value	Unit
PV arrays		
Total rated capacity, $P_{s,PV}$	100	kW
Investment cost, $C_{PV,inv}$	2500	$/kW
Working lifetime, L_{PV}	20	year
Wind turbines		
Total rated capacity, $P_{r,WT}$	50	kW
Investment cost, $C_{WT,inv}$	2300	$/kW
Working lifetime, L_{WT}	20	year
Diesel engine		
Rated power, $P_{D,r}$	20	kW
Minimize power output coefficient, θ_D	0.3	–
Minimum uptime, $d_{on,l}$	1	h
Maximum uptime, $d_{on,u}$	10	h
Minimum downtime, $d_{off,l}$	1	h
Maximum lifting capacity, $P_{D,up,\max}$	20	kW/h
Maximum lowering capacity, $P_{D,dw,\max}$	20	kW/h
Investment cost, $C_{D,inv}$	1000	$/kW
Working lifetime, L_D	24,000	h
Fuel price, $V_{D,F}$	0.9	$/L
Start-up cost, $V_{D,S}$	1.2	$
Battery		
Rated capacity, C_B	200	kWh
Maximum charging power, $P_{B,ch,\max}$	40	kW
Maximum discharging power, $P_{B,dch,\max}$	40	kW
Charging efficiency, $\lambda_{B,ch}$	0.95	–
Discharging efficiency, $\lambda_{B,dch}$	0.95	–
Allowable SOC range, $SOC_{B,\min} \sim SOC_{B,\max}$	0.2–0.9	–
Investment cost, $C_{B,inv}$	150	$/kWh
Energy throughput per capacity, $L_{B,thr}$	3400	kWh
Supercapacitor		
Rated capacity, C_S	12	kWh
Maximum charging power, $P_{S,ch,\max}$	24	kW
Maximum discharging power, $P_{S,dch,\max}$	24	kW
Charging efficiency, $\lambda_{S,ch}$	0.98	–
Discharging efficiency, $\lambda_{S,dch}$	0.98	–
Allowable SOC range, $SOC_{S,\min} \sim SOC_{S,\max}$	0.05–0.95	–
Optimal SOC, $SOC_{S,opt}$	0.5	–
Trigger threshold, θ_S	0.3	–
Recovery coefficient, ξ_{PP}	0.2	–
Investment cost, $C_{S,inv}$	3600	$/kWh
Working lifetime, L_S	25	year

4.1. Simulation setups

We assumed that the 24-h RH is divided into $T = 48$ equal time intervals (i.e., optimization time resolution Δt and MI are both 0.5 h). To reflect the power fluctuations, we assume that there are $K = 5$ equal time intervals in Δt (i.e., real-time time resolution is $\Delta k = 0.1$ h) for actual RESs generation, load demand, and grid power.

The MG system can purchase energy from or sell it back to the main grid. The time-of-use (TOU) price is shown in Table 1, and the maximum grid-connected buying and selling power limits are both 110 kW. The basic parameters of MG for the simulations are specified in Table 2. The penalty factors ρ and ξ_F are set to 0.005 and 2, respectively. The

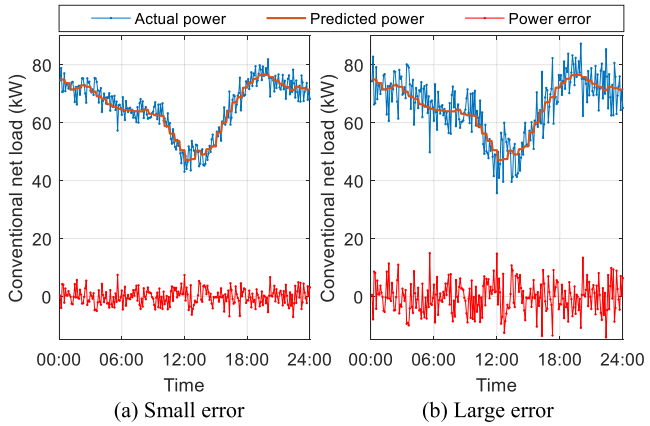

Fig. 3. The actual power curves of CNL and their prediction results.

Table 3
MG configuration in six test scenarios.

Scenario	Type of fluctuations	Configuration		
		Strategy	ESS	Smoothing resources
S1	Small	DAOS	BESS	Grid
S2	Small	BROS	HESS	SC > Grid
S3	Small	NROS	HESS	HCL > SC > Battery > Grid
S4	Large	DAOS	BESS	Grid
S5	Large	BROS	HESS	SC > Grid
S6	Large	NROS	HESS	HCL > SC > Battery > Grid

maximum working power of HCL $P_{T,\max}$ is 15 kW. In addition, the predefined indoor temperature range is from 20 °C to 25 °C, the optimal indoor temperature range is from 23 °C to 24 °C, the thermal resistance of building shell R_T is 6 °C/kW, and the heat capacity of indoor air C_{air} is 0.525 kWh/°C.

The initial MG states are as follows: the initial SOCs for supercapacitor and battery are 0.5 and 0.2. The initial grid power drawn from the main grid is 90 kW, the initial DE power is 0 kW, and the initial indoor temperature is 23 °C.

The CNL demand in a day with a 6-min time resolution is used for simulation analysis. The assumed actual power profiles with small and large power fluctuations and their prediction results for CNL are shown in Fig. 3. As it can be seen, power errors (unpredicted power fluctuations) were assumed to be normal in distribution [24,42].

Six test scenarios for simulation studies are specified in Table 3. There are three strategies, including deterministic day-ahead optimization strategy (DAOS), basic rolling optimization strategy (BROS), and novel rolling optimization strategy (NROS). Noted that the DAOS is based on previous work [40], and the design of BROS is used study [29] as a reference. The three strategies are applied in the scenarios with small and large power fluctuations, respectively.

Remark 3. Scenario 1 (S1) and Scenario 4 (S4) are the basic scenarios for performance comparison. S1 and S4 only configure the battery, and the battery ESS (BESS) only participates in DAOS. Thus, unpredicted power fluctuations are only balanced through the main grid in real time.

Remark 4. The BROS with the energy trigger mechanism for SC is applied in Scenario 2 (S2) and Scenario 5 (S5). In these two scenarios, SC is preferred to smooth out unpredictable power fluctuations. Moreover, Scenario 3 (S3) and Scenario 6 (S6) can fully demonstrate the superior performance of the proposed NROS in this paper.

The two new operation indicators are presented to quantitatively evaluate the operating performance in the six test scenarios. They are including daily operation cost (DOC) and average power fluctuations (APF) based on actual daily power data, which are expressed as

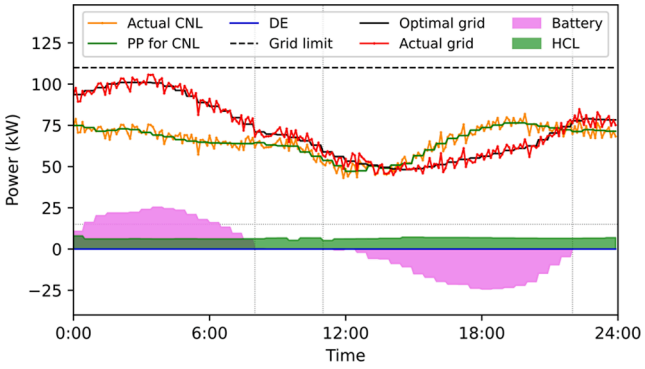

Fig. 4. Optimal results of DAOS in S1 with small power fluctuations.

$$DOC = C_{PV}^{RH} + C_{WT}^{RH} + \sum_{k\in \text{one day}} \left(C_B^k + C_S^k + C_D^k\right) + \Delta k \sum_{k\in \text{one day}} \left(P_{G,B}^k V_{G,B}^k - P_{G,S}^k V_{G,S}^k\right) + \rho \sum_{k\in \text{one day}} \Delta P_G^{2,k} \tag{44}$$

$$APF = \sqrt{\frac{\Delta k}{24} \sum_{k\in \text{one day}} \Delta P_G^{2,k}} \tag{45}$$

4.2. Simulation results for small power fluctuations

We first simulate DAOS, BROS, and NROS under small power fluctuations, and then analyze the simulation results from the perspectives of economy and volatility.

1) *Simulation Result of Scenario 1:* MG system in S1 with small power fluctuations performs the deterministic DAOS. Considering the main grid has set the maximum grid-connected power limits, the limits need to reserve power margin to avoid the grid-connected power exceeding the limits.

The DAOS is a typical deterministic scheduling strategy, which collects the day-ahead forecast data and system parameters in advance. The simulation result of DAOS in S1 is shown in Fig. 4. It shows that the actual CNL has a lot of unpredicted power fluctuations, but the predicted CNL and the optimal results with 0.5-h time resolution is a continuous step value. In the optimization process, HCL and CNL are powered by the main grid, battery, or DE. The battery is also used to participate in demand response. It is charged during the low electricity price periods and discharged during the high electricity price periods.

To ensure that the optimal results of DAOS can be effectively implemented, the unpredictable power fluctuations are smoothed only by the main grid. During the actual operation of MG, the actual grid power is obtained by the optimal solution of DAOS plus the unpredicted power fluctuations of the CNL.

In S1, the index of DOC is $281.9232, which includes a penalty cost $20.0761 for grid-connected power fluctuations. The index of APF is 4.0902 kW. In this scenario, the main grid needs to compensate for the power fluctuations in real time. However, as the number of microgrids increases, this scheduling strategy is not conducive to economic and stable operations of the MG system and the main grid.

2) *Simulation Result of Scenario 2:* S2 adopts the BROS, and it is equipped with a battery-supercapacitor HESS. The objective of this scenario is to reduce unpredictable grid-connected power fluctuations as well as improve the dispatch economy of MG. The optimization process at each time interval only involves a rolling horizon in the future 24 h from the current moment. When the time comes to the next time interval, this rolling horizon moves forward for 30 min. As long as

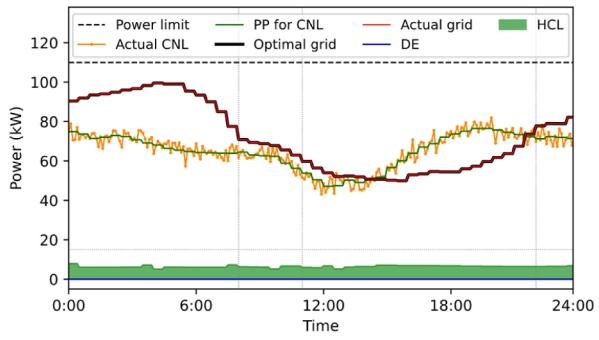

(a) Power profiles of MG system

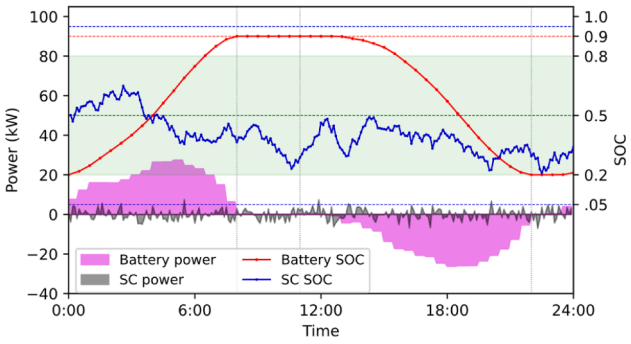

(b) Battery and SC operation of MG system

Fig. 5. Optimal results of BROS in S2 with small power fluctuations.

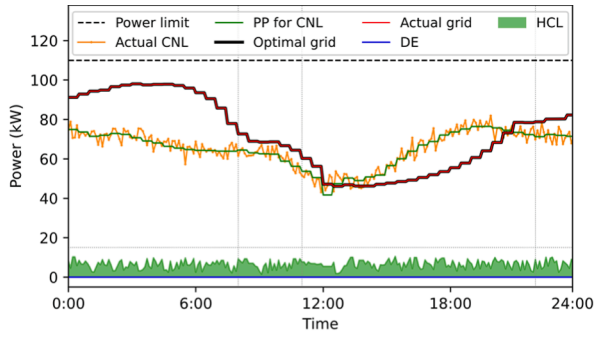

(a) Power profiles of MG system

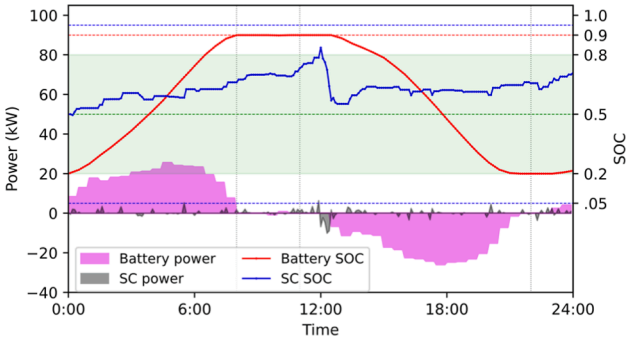

(b) Battery and SC operation of MG system

Fig. 6. Optimal results of NROS in S3 with small power fluctuations.

the CNL changes are acquired 30 min in advance, the BROS can perform feedback correction on the optimization results. The simulation result of BROS in S2 with small power fluctuations is shown in Fig. 5.

According to Fig. 5**a**, we can see that benefiting from the participation of SC in smoothing power fluctuations, the actual grid power can be consistent with the optimized grid power. Moreover, the minimization of grid-connected power fluctuations is one of the optimization goals, which makes the changes of grid-connected power more gradual. This strategy effectively avoids the sudden change of grid-connected power caused by battery charging or discharging.

Besides, it can be seen in Fig. 5**b** that the SC smooths the unpredictable power fluctuations in the CNL in real time. The simulation results also show that the battery participates in an economic dispatch, and partially smooths the grid-connected power fluctuations caused by economic dispatch. Since the scenario adopts the small power fluctuations obeyed the normal distribution, the SOC of the SC in a day is always kept within the optimal range of 0.2–0.8.

In S2, the index of DOC is $268.4503 (including a penalty cost $1.6179 for grid-connected power fluctuations and a grid power cost $197.1967); The index of APF is 1.1611 kW. Compared with S1, the DOC of S2 has dropped by 4.78%, and the grid-connected power fluctuations have dropped by 71.61%. In fact, the online feedback correction of BROS can better adapt to the actual MG system and improve the scheduling accuracy of the EMS. Simulation analysis shows that MG combined HESS can not only improve the dispatching economy, but also greatly reduce grid-connected power fluctuations.

3) *Simulation Result of Scenario 3:* S3 adopts the proposed NROS. In this scenario, the HCL, HESS and the main grid are used as resources for smoothing power fluctuations. They are applied to real-time smoothing power fluctuations according to the set priority. The simulation result of NROS in S3 with small power fluctuations is shown in Fig. 6.

Fig. 6**a** shows the power curves of grid-connected power, HCL power, and DE power. Since the HCL is the highest priority smoothing resource, HCL is first used to adjust power in real time for responding to power fluctuations. Therefore, we can find that the power curve of HCL is also fluctuating. The magnitude of fluctuations depends on the acceptable indoor temperature range 20–25 °C set in advance.

However, the remaining power capacity of HCL is variable and limited. Some large-amplitude power fluctuations still require SC to participate in smoothing, which can be seen from Fig. 6**b.** It can be seen from the figure that the running time for the SC to participate in power fluctuations smoothing is reduced to about one-third of the simulation day.

We also can find that the SOC of SC exceeds the optimal range at 12:00, which triggers the energy trigger mechanism for SC. This indicates that the SC needs to be discharged, and then the upcoming value of point prediction is revised down. After the process of forced discharge, the SC is restored to near the optimal SOC 0.5.

As a typical flexible load, the HCL has the flexibility to adjust working state for power regulation. In this simulation scenario, the HCL is playing a role in power regulation as virtual energy storage. In S3, the index of DOC is $265.9467 (including the penalty cost $1.9678 for grid-connected power fluctuations and the grid power cost $197.5257), and the index of APF is 1.2806 kW. Compared with S2, the DOC of S3 is further reduced by 0.93% ($2.5036), and this is because the flexible load HCL replaces the SC for power fluctuations smoothing. Therefore, our proposed NROS is more economic and stable for operation in MG with small power fluctuations than the optimization strategies of DAOS and BROS.

4.3. Simulation results for large power fluctuations

To verify the performance of the proposed strategy more comprehensively, we further applied the three optimization strategies to the simulation environment with large power fluctuations.

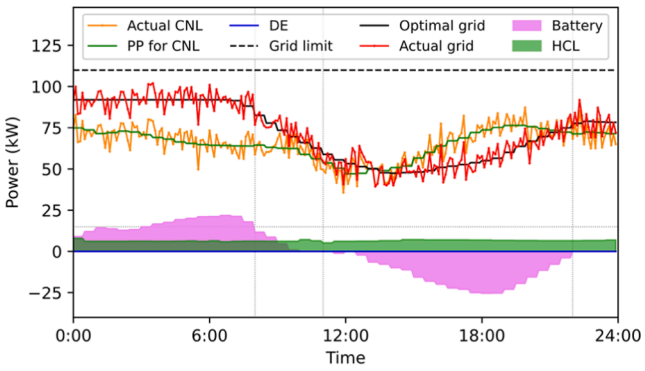

Fig. 7. Optimal results of DAOS in S4 with large power fluctuations.

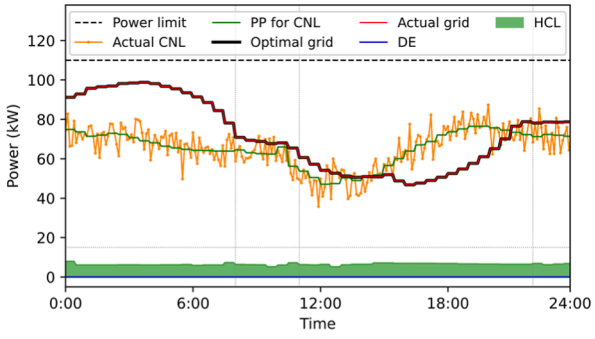

(a) Power profiles of MG system

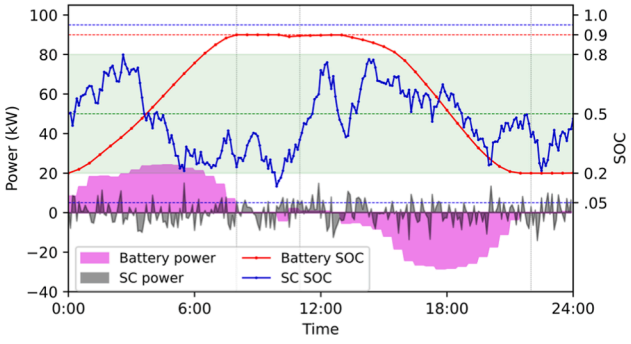

(b) Battery and SC operation of MG system

Fig. 8. Optimal results of BROS in S5 with large power fluctuations.

1) *Simulation Result of Scenario 4:* The simulation result of DAOS in S4 with large power fluctuations is shown in Fig. 7, in which the unpredicted power fluctuations will be directly balanced by the main grid. This will not only cause harmonic pollution to the main grid, but also greatly increase the penalty fee for grid-connected power fluctuations of the MG. In S4, the index of DOC is $337.4106 (including a penalty cost $74.8033 for grid-connected power fluctuations and a grid power cost $197.9398), and the index of APF is 7.8953 kW. Compared with S1, the main reason for the substantial increase in the DOC of S4 is the failure to absorb the large power fluctuations locally.
2) *Simulation Result of Scenario 5:* In this scenario, we consider that the SC and the main grid are used as smoothing resources to balance large power fluctuations. The SC with high power density has enough capacity to smooth out the large power fluctuations in real time. Fig. 8 shows the simulation result of BROS. Fig. 8**a** indicates that although there are large power fluctuations in the MG, with the participation of SC and the cooperation of the designed energy trigger mechanism for SC, the fluctuations of grid-connected power

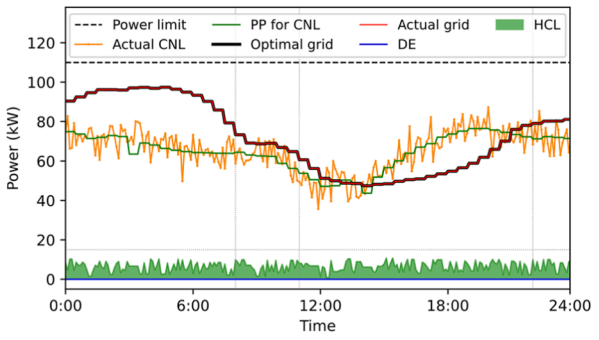

(a) Power profiles of MG system

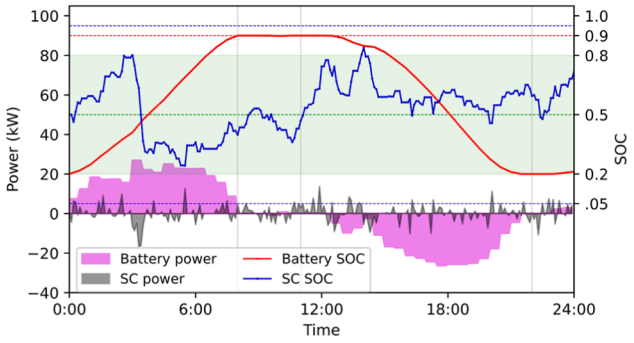

(b) Battery and SC operation of MG system

Fig. 9. Optimal results of NROS in S6 with large power fluctuations.

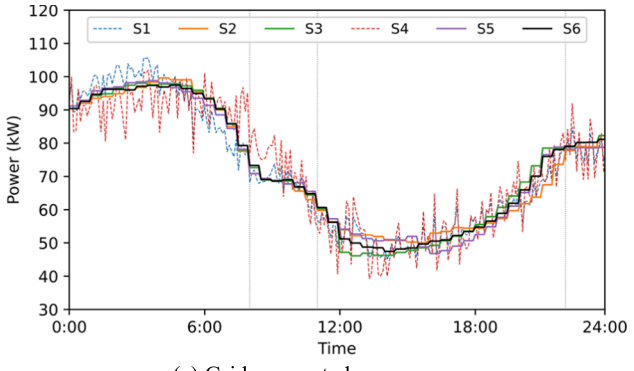

(a) Grid-connected power curves

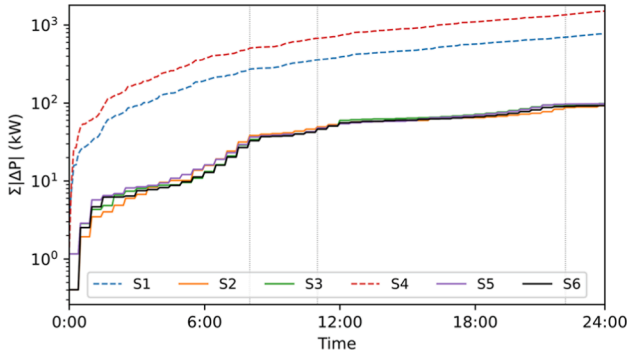

(b) Cumulative power fluctuations

Fig. 10. Comparison of grid-connected power among six scenarios.

can be effectively absorbed by the SC. Fig. 8**b** shows the operation results of battery and SC. It is indicated that the SOC and power of SC vary with the changing power fluctuations. Under the action of the designed energy trigger mechanism, the SOC is kept within the

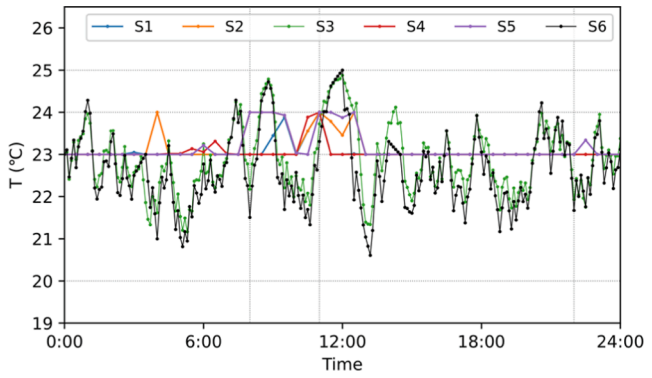

Fig. 11. Indoor temperature curves among six scenarios.

optimal range set. In S5, the index of DOC is $268.8501, which is 20.32% lower than that of S4.

3) *Simulation Result of Scenario 6:* Similarly, the simulation result of NROS in S6 with large power fluctuations is shown in Fig. 9. From Fig. 9**a**, we can observe that under the premise of ensuring a feasible indoor temperature range, the HCL uses the remaining power capacity to participate in smoothing power fluctuations. Since the remaining capacity of the HCL is not enough to smooth the large-scale power fluctuations, the reduction in the running time of SC in S6 is about one-third compared with S5, which can be seen from Fig. 9**b**.

In S6, the index of DOC is $267.3823 (including a penalty cost $1.6094 for grid-connected power fluctuations and a grid cost $197.8362), and the index of APF is 1.1581 kW. Compared with S5, the drop in DOC is very small, because the large power fluctuations smoothing also requires the participation of SC.

4.4. Performance comparison among six scenarios

Furthermore, to comprehensively clarify the advantages of the proposed optimization strategy, we compared and analyzed the simulation results of these six scenarios in detail.

Fig. 10 shows the grid-connected power curves and the cumulative power fluctuations, in which S1 and S4 both adopt a deterministic day-ahead optimization strategy. As can be seen from the figures, smoothing power fluctuations through the main grid will cause a large number of unpredictable power fluctuations to be directly injected into the main grid. This is also the main reason why the cumulative power fluctuations are much larger than in other scenarios. However, we can find that the grid-connected power curves of S2, S3, S5, and S6 are very close. This is because these power fluctuations are locally absorbed by the microgrid.

In this paper, the optimal indoor temperature range is 23–24 °C, and the predefined indoor temperature range is 20–25 °C. Therefore, the indoor temperature in S1, S2, S4, and S5 is maintained between 23 °C and 24 °C throughout the day, which can be seen from Fig. 11. However, the HCLs of S3 and S6 use the remaining power capacity to participate in the smoothing of power fluctuations. This improves the dispatching economy of MG system, but it increases the fluctuations of the indoor temperature.

Table 4 comprehensively summarizes the performance indicators of the above six simulation scenarios. We can conclude that the cost difference among six scenarios is mainly reflected in the cost of SC, and the penalty for grid-connected power fluctuations. The optimization strategies of BROS and NROS make a trade-off between economy and volatility according to the set goals. In general, selecting NROS can effectively improve the economic benefit and reduce the grid-connected power fluctuations of the MG. From the simulation results, whether it is small or large power fluctuations, the economy of NROS is the best one.

This paper proposes an optimization strategy to reduce the impact of power errors on scheduling optimization. Considering the flexible load to participate in smoothing power fluctuations, the novel rolling optimization strategy improves the operating economy while reducing the negative impact of power fluctuations on the grid.

5. Conclusion and future work

5.1. Conclusion

With an increasing of distributed renewable energy sources and grid-connected microgrids, harmonics pollution is increasingly serious in power systems. To solve the problem of grid-connected power fluctuations mainly caused by power prediction errors, this paper proposes a novel rolling optimization strategy (ROS) considering grid-connected power fluctuations smoothing. The supercapacitor-battery energy storage system is introduced to simultaneously achieve economic dispatching and power fluctuations smoothing. Moreover, as a flexible load, the heating/cooling load can be used as virtual energy storage to participate in power regulation. To maintain the supercapacitor with limited capacity in an optimal energy range, an energy trigger mechanism is also designed for the supercapacitor. Finally, we integrate the energy trigger mechanism and the priority-based power fluctuations smoothing method into the rolling optimization strategy to form the novel ROS. The optimization objective of the proposed novel ROS is to minimize the total operating cost of the microgrid. Simulation results of six scenarios show that the proposed novel ROS has advantages in economy and power fluctuations smoothing over traditional deterministic energy scheduling strategies. Besides, adding flexible loads to participate in dispatching can further improve the ability to smooth power fluctuations.

5.2. Future work

In future work, an improved optimization method will be considered to improve the computational efficiency for this complex mixed-integer nonlinear programming problem. In addition, the rolling forecast method is also an interesting research work, which can better reflect the advantages of rolling optimization.

CRediT authorship contribution statement

Shenglin Li: Conceptualization, Methodology, Software, Validation, Writing – original draft, Writing – review & editing. **Jizhong Zhu:**

Table 4
Performance evaluation indicators in the test scenarios.

Scenario	Type of fluctuations	Strategy	Daily cost for each module ($)							APF (kW)	DOC ($)	Saving (%)
			PV	WT	Battery	SC	DE	Grid	Fluctuation			
S1	Small	DAOS	34.2466	15.7534	14.6504	–	0	197.1967	20.0761	4.0902	281.9232	–
S2	Small	BROS	34.2466	15.7534	14.7669	4.7342	0	197.3313	1.6179	1.1611	268.4503	4.78
S3	Small	NROS	34.2466	15.7534	14.8751	1.5781	0	197.5257	1.9678	1.2806	265.9467	5.67
S4	Large	DAOS	34.2466	15.7534	14.6675	–	0	197.9398	74.8033	7.8953	337.4106	–
S5	Large	BROS	34.2466	15.7534	14.7947	4.7342	0	197.6110	1.7102	1.1938	268.8501	20.32
S6	Large	NROS	34.2466	15.7534	14.8397	3.0970	0	197.8362	1.6094	1.1581	267.3823	20.75

Conceptualization, Methodology, Writing – review & editing. **Hanjiang Dong:** Supervision, Visualization, Writing – review & editing. **Haohao Zhu:** Investigation, Data curation, Validation, Writing – review & editing. **Junwei Fan:** Investigation, Formal analysis, Validation, Supervision.

Declaration of Competing Interest

The authors declare that they have no known competing financial interests or personal relationships that could have appeared to influence the work reported in this paper.

Acknowledgement

This work was financially funded in part by the Science and Technology Planning Project of Guangdong Province of China (2020A0505100004), and in part by the National Natural Science Foundation of China (52177087).

References

[1] Esen M, Yuksel Y. Experimental evaluation of using various renewable energy sources for heating a greenhouse. Energy Build 2013;65:340–51. https://doi.org/10.1016/j.enbuild.2013.06.018.
[2] Li Z, Zhang H, Meng J, Long Y, Yan Y, Li M, et al. Reducing carbon footprint of deep-sea oil and gas field exploitation by optimization for Floating Production Storage and Offloading. Appl Energy 2020;261:114398. https://doi.org/10.1016/j.apenergy.2019.114398.
[3] IRENA. Renewable power generation costs in 2019. International Renewable Energy Agency; 2020. https://www.irena.org/publications/2020/Jun/Renewable-Power-Costs-in-2019.
[4] Cagnano A, De Tuglie E, Mancarella P. Microgrids: overview and guidelines for practical implementations and operation. Appl Energy 2020;258:114039. https://doi.org/10.1016/j.apenergy.2019.114039.
[5] Kiptoo MK, Lotfy ME, Adewuyi OB, Conteh A, Howlader AM, Senjyu T. Integrated approach for optimal techno-economic planning for high renewable energy-based isolated microgrid considering cost of energy storage and demand response strategies. Energy Conv Manag 2020;215:112917. https://doi.org/10.1016/j.enconman.2020.112917.
[6] Atia R, Yamada N. Sizing and analysis of renewable energy and battery systems in residential microgrids. IEEE Trans Smart Grid 2016;7(3):1204–13. https://doi.org/10.1109/TSG.2016.2519541.
[7] Jia K, Chen Y, Bi T, Lin Y, Thomas D, Sumner M. Historical-data-based energy management in a microgrid with a hybrid energy storage system. IEEE Trans Ind Inform 2017;13(5):2597–605. https://doi.org/10.1109/tii.2017.2700463.
[8] Zhong Q, Hornik T. Cascaded current–voltage control to improve the power quality for a grid-connected inverter with a local load. IEEE Trans Ind Electron 2013;60(4):1344–55. https://doi.org/10.1109/TIE.2012.2187415.
[9] Zhang F, Mu L. A fault detection method of microgrids with grid-connected inverter interfaced distributed generators based on the PQ control strategy. IEEE Trans Smart Grid 2019;10(5):4816–26. https://doi.org/10.1109/TSG.2018.2868967.
[10] Ghorbani N, Kasaeian A, Toopshekan A, Bahrami L, Maghami A. Optimizing a hybrid wind-PV-battery system using GA-PSO and MOPSO for reducing cost and increasing reliability. Energy 2018;154:581–91. https://doi.org/10.1016/j.energy.2017.12.057.
[11] Li S, Zhu J, Chen Z, Luo T. Double-layer energy management system based on energy sharing cloud for virtual residential microgrid. Appl Energy 2021;282:116089. https://doi.org/10.1016/j.apenergy.2020.116089.
[12] Liu C, Wang X, Wu X, Guo J. Economic scheduling model of microgrid considering the lifetime of batteries. IET Gener Transm Distrib 2017;11(3):759–67. https://doi.org/10.1049/iet-gtd.2016.0772.
[13] Hossain MA, Pota HR, Hossain MJ, Blaabjerg F. Evolution of microgrids with converter-interfaced generations: challenges and opportunities. Int J Electr Power Energy Syst 2019;109:160–86. https://doi.org/10.1016/j.ijepes.2019.01.038.
[14] Mirzapour F, Lakzaei M, Varamini G, Teimourian M, Ghadimi N. A new prediction model of battery and wind-solar output in hybrid power system. J Ambient Intell Humaniz Comput 2019;10(1):77–87. https://doi.org/10.1007/s12652-017-0600-7.
[15] Mohammadi M, Talebpour F, Safaee E, Ghadimi N, Abedinia O. Small-scale building load forecast based on hybrid forecast engine. Neural Process Lett 2018;48(1):329–51. https://doi.org/10.1007/s11063-017-9723-2.
[16] Ebrahimian H, Barmayoon S, Mohammadi M, Ghadimi N. The price prediction for the energy market based on a new method. Ekon Istraz 2018;31(1):313–37. https://doi.org/10.1080/1331677X.2018.1429291.
[17] Zhou B, Meng Y, Huang W, Wang H, Deng L, Huang S, et al. Multi-energy net load forecasting for integrated local energy systems with heterogeneous prosumers. Int J Electr Power Energy Syst 2021;126:106542. https://doi.org/10.1016/j.ijepes.2020.106542.
[18] Peng X, Wang H, Lang J, Li W, Xu Q, Zhang Z, et al. EALSTM-QR: interval wind-power prediction model based on numerical weather prediction and deep learning. Energy 2021;220:119692. https://doi.org/10.1016/j.energy.2020.119692.
[19] Wei Q, Liu D, Lewis FL, Liu Y, Zhang J. Mixed iterative adaptive dynamic programming for optimal battery energy control in smart residential microgrids. IEEE Trans Ind Electron 2017;64(5):4110–20. https://doi.org/10.1109/TIE.2017.2650872.
[20] Park L, Jang Y, Cho S, Kim J. Residential demand response for renewable energy resources in smart grid systems. IEEE Trans Ind Informat 2017;13(6):3165–73. https://doi.org/10.1109/TII.2017.2704282.
[21] Zhao Bo, Qiu H, Qin R, Zhang X, Gu W, Wang C. Robust optimal dispatch of AC/DC hybrid microgrids considering generation and load uncertainties and energy storage loss. IEEE Trans Power Syst 2018;33(6):5945–57. https://doi.org/10.1109/TPWRS.2018.2835464.
[22] Nguyen TA, Crow ML. Stochastic optimization of renewable-based microgrid operation incorporating battery operating cost. IEEE Trans Power Syst 2016;31(3):2289–96. https://doi.org/10.1109/TPWRS.2015.2455491.
[23] Yu D, Ghadimi N. Reliability constraint stochastic UC by considering the correlation of random variables with Copula theory. IET Renew Power Gener 2019;13(14):2587–93. https://doi.org/10.1049/iet-rpg.2019.0485.
[24] Huang Y, Wang L, Guo W, Kang Q, Wu Q. Chance constrained optimization in a home energy management system. IEEE Trans Smart Grid 2018;9(1):252–60. https://doi.org/10.1109/TSG.2016.2550031.
[25] Yang X, Zhang Y, Wu H, He H. An event-driven ADR approach for residential energy resources in microgrids with uncertainties. IEEE Trans Ind Electron 2019;66(7):5275–88. https://doi.org/10.1109/TIE.2018.2868019.
[26] Yang X, Zhang Y, He H, Ren S, Weng G. Real-time demand side management for a microgrid considering uncertainties. IEEE Trans Smart Grid 2019;10(3):3401–14. https://doi.org/10.1109/TSG.2018.2825388.
[27] Li S, Yang J, Song W, Chen An. A real-time electricity scheduling for residential home energy management. IEEE Internet Things J 2019;6(2):2602–11. https://doi.org/10.1109/JIOT.2018.2872463.
[28] Zhao H, Wu Q, Hu S, Xu H, Rasmussen CN. Review of energy storage system for wind power integration support. Appl Energy 2015;137:545–53. https://doi.org/10.1016/j.apenergy.2014.04.103.
[29] Ju C, Wang P, Goel L, Xu Y. A two-layer energy management system for microgrids with hybrid energy storage considering degradation costs. IEEE Trans Smart Grid 2018;9(6):6047–57. https://doi.org/10.1109/TSG.2017.2703126.
[30] Sharma RK, Mishra S. Dynamic power management and control of a PV PEM fuel-cell-based standalone ac/dc microgrid using hybrid energy storage. IEEE Trans Ind Appl 2018;54(1):526–38. https://doi.org/10.1109/tia.2017.2756032.
[31] Jin X, Mu Y, Jia H, Wu J, Jiang T, Yu X. Dynamic economic dispatch of a hybrid energy microgrid considering building based virtual energy storage system. Appl Energy 2017;194:386–98. https://doi.org/10.1016/j.apenergy.2016.07.080.
[32] Veers P, Dykes K, Lantz E, Barth S, Bottasso CL, Carlson O, et al. Grand challenges in the science of wind energy. Science 2019;366(6464). https://doi.org/10.1126/science:aau2027.
[33] Hossain MA, Pota HR, Squartini S, Zaman F, Guerrero JM. Energy scheduling of community microgrid with battery cost using particle swarm optimisation. Appl Energy 2019;254:113723. https://doi.org/10.1016/j.apenergy.2019.113723.
[34] Ahmadi M, Rosenberger JM, Lee WJ, Kulvanitchaiyanunt A. Optimizing load control in a collaborative residential microgrid environment. IEEE Trans Smart Grid 2015;6(3):1196–207. https://doi.org/10.1109/tsg.2014.2387202.
[35] Yang D, Jiang C, Cai G, Huang N. Optimal sizing of a wind/solar/battery/diesel hybrid microgrid based on typical scenarios considering meteorological variability. IET Renew Power Gener 2019;13(9):1446–55. https://doi.org/10.1049/iet-rpg.2018.5944.
[36] Zhao B, Zhang X, Chen J, Wang C, Guo L. Operation optimization of standalone microgrids considering lifetime characteristics of battery energy storage system. IEEE Trans Sustain Energ 2013;4(4):934–43. https://doi.org/10.1109/tste.2013.2248400.
[37] Jenkins DP, Fletcher J, Kane D. Lifetime prediction and sizing of lead-acid batteries for microgeneration storage applications. IET Renew Power Gener 2008;2(3):191–200. https://doi.org/10.1049/iet-rpg:20080021.
[38] He F, Zhou J, Mo Li, Feng K, Liu G, He Z. Day-ahead short-term load probability density forecasting method with a decomposition-based quantile regression forest. Appl Energy 2020;262:114396. https://doi.org/10.1016/j.apenergy.2019.114396.
[39] Silvente J, Kopanos GM, Pistikopoulos EN, Espuna A. A rolling horizon optimization framework for the simultaneous energy supply and demand planning in microgrids. Appl Energy 2015;155:485–501. https://doi.org/10.1016/j.apenergy.2015.05.090.
[40] Erdinc O, Paterakis NG, Mendes TDP, Bakirtzis AG, Catalao JPS. Smart household operation considering bi-directional EV and ESS utilization by real-time pricing-based DR. IEEE Trans Smart Grid 2015;6(3):1281–91. https://doi.org/10.1109/TSG.2014.2352650.
[41] Gurobi 9.0 Optimization. Accessed: Mar. 10, 2021. [Online]. Available: http://www.gurobi.com.
[42] Liu N, Yu X, Wang C, Li C, Ma L, Lei J. Energy-sharing model with price-based demand response for microgrids of peer-to-peer prosumers. IEEE Trans Power Syst 2017;32(5):3569–83. https://doi.org/10.1109/TPWRS.2017.2649558.

Shenglin Li received the B.S. and M.S. degree both from Shanghai University of Electric Power, Shanghai, China, in 2016 and 2019, respectively. He is currently working toward the Ph.D. degree with the School of Electric Power Engineering, South China University of Technology, Guangzhou, China. His current research interests include the energy management of renewable energy microgrids and energy sharing.

Jizhong Zhu (Corresponding author) was born in Sichuan, China in 1966. He received the B.S., M.S., and Ph.D. degrees in electrical engineering from Chongqing University, Chongqing, China, in 1985, 1987, and 1990, respectively. His work experience includes Chongqing University; Brunel University, U.K.; National University of Singapore; Howard University; ALSTOM Grid Inc. and SEPRI, CSG. He is a Fellow of IEEE and a Professor at the School of Electric Power Engineering, South China University of Technology. His research interests include power system operation and control, smart grid, microgrid, virtual power plant, electric vehicle, renewable energy application and integrated smart energy system.

Hanjiang Dong received the B.S. degree in Electrical Engineering and its Automation from Jinan University, Guangzhou, China, in 2020. He is currently working toward the Ph.D. degree with the School of Electric Power Engineering, South China University of Technology, Guangzhou, China. His current research interests include artificial intelligence and data analysis in modern power system.

Haohao Zhu received the B.S. from Nanchang University, Nanchang, China, in 2020. He is currently working toward the M.S. degree with the School of Electric Power Engineering, South China University of Technology, Guangzhou, China. His current research interests include optimization and operation of the integrated electricity and heat systems.

Junwei Fan received the B.S. degree in Electrical Engineering and Automation from China University of Mining and Technology, Xuzhou, China, in 2020. He is currently working toward the M.S. degree with the School of Electric Power Engineering, South China University of Technology, Guangzhou, China. His current research interests include application of blockchain in carbon market and peer-to-peer transactions.